PREPARATION AND CHARACTERIZATION OF ACTIVATED CARBON FROM *Pilliostigma thonningii, Hildergardia barteri, Perqutinia nigrecens* AND THE COMPOSITE.

Etong, D. I.[1] and Abdus-Salam, N[2]

[1]Department of Chemical and Biochemical Sciences, Fed. Poly. P.M.B. 420, Offa, Kwara State, Nigeria.
[2]Department of Chemistry, University of Ilorin, P.M.B. 1515, Ilorin, Nigeria.
Corresponding Author: danieletong291@gmail.com

Abstract.

In this study, activated carbon was prepared from three different biomass *Pilliostigma thonningii (PSH), Hildergardia barteri (HB), Perqutinia nigrecens (PNS)* and composited with magnetite. It was characterized physico – chemically and instrumentally using FTIR, SEM, CHN, EDX and BET. The percentage yield was 23.98 for HB, 32.04 for PSH and 32.12 for PNS at 400 ºC. The iodine number was 850.0 ± 10; 900.0 ± 20 and 950.0 ± 25 mg/g for PSH, PNS and HB respectively. The pH_{pzc} was HB 7.5, PSH 4.1 and PNS 4.9. The CHN analysis gave percentage carbon 68.42 (PNS), 69.42 (PSH) and 72.27 (HB) %. The FTIR spectroscopy revealed C≡C, C=O, C=C and CH for the activated carbon, while the composite of the activated carbon revealed C≡C, conjugated C=C for Magnetite *Perqutinia nigrecens* (MPNS) and Fe-O stretching and bending vibrations in the entire composite. The disappearance and appearance of some bands in the composite signifies successful compositing of the activated carbon and the magnetite.

Keyword: *Pilliostigma thonningii, Hildergardia barteri , Perqutinia nigrecens,* Magnetite, Adsorbent.

Introduction:

In developing nations, the activated carbon (AC) requirements are met by importation in enormous quantity at a very high cost depleting their foreign reserves. Annually, large quantities of agricultural by – products, which can be used for activated carbon production to meet local demands, are generated. It will be a value added product and resource for other industries, if activated carbon production technology is developed to harness these by-products.

Environmental pollution has recently become a severe problem worldwide (Paul *et al.*, 2011). Some of the most hazardous chemical compounds found in industrial effluents are dyes and heavy metals and they need to be treated since their presence in water bodies reduces light penetration precluding the photosynthesis of aqueous flora (Royer *et al.*, 2009). Dyes are also aesthetically objectionable for drinking and other purposes (Royer *et al.*, 2010) and can result to allergy, dermatitis, skin irritation (Brookstein, 2009) and also provoke cancer (Lima *et al.,*2007) and mutation in humans (Royer *et al.,* 2010).

Hyper filtration, oxidation, adsorption, floatation, coagulation and biological treatment are the conventional methods of color removal from industrial effluents (Asiagwu *et al.,* 2012). Among the treatment options, adsorption appears to have considerable potential for the removal of color and heavy metals from industrial effluents. For micro-pollutants removal adsorption onto activated carbon is an acceptable process.

Activated carbon is a solid porous and black carbonaceous material that has an essentially graphitic structure (Abdus-Salam and Buhari, 2014). The oxidation of the carbon surface and the removal of all non-carbon impurities distinguished it from elemental carbon. Also activated carbon contains physical features such as pore volume and large internal surface area. It has high capacity for adsorbing chemicals from gases or liquids because of the large surface area. The adsorptive nature comes from the extensive internal pore structure that develops during the activation procedure. Few of the adsorptive materials that have been tested for the treatment of wastewater include biopolymers such as chitosan beads (Chiou and Li, 2002), activated carbon (Abdus-Salam and Buhari, 2014), quaternary chitosan (Rosa *et al.,* 2008) and agricultural by-products (Wang *et al.,* 2008).

The increased interest in the use of agricultural based precursors for the preparation of activated carbon is partly because it is a way of recycling agricultural wastes which could otherwise constitute environmental pollution, particularly as it relates to solid waste management, its low cost and renewable source. The adsorptive properties of activated carbon prepared from different agricultural base materials varies widely, which is essentially due to the optimization of preparation conditions (Torregrosa-Macia *et al.,* 1997). Chemical activation process can solely produce activated carbon with a relatively wide pore size distribution (Torregrosa-Macia *et al.,* 1997). The use of gases such as CO/CO_2 or steam, physical activation, can further enhance the adsorbents pore structure due to partial oxidation of the carbonized materials.

In order to reduce preparation cost, the use of low cost starting materials (industrial or agricultural residues) for activated carbon preparation has emerged as a potential alternative (Bhatnagar and Sillanpaa, 2010). The conversion of agricultural waste into low cost adsorbents also added value to the residues and solve the problem of biomass disposal, besides the cost reduction. Agricultural waste-based carbon is advantageous in exhibiting low ash content, reasonable hardness and high surface area and/or adequate porous structures (Bhatnagar and Sillanpaa, 2010). The cost, its availability and purity affect the choice of activated carbon precursor largely but the preparatory process and intended application of the product are also important consideration. Therefore, evaluation of biomass is getting increased attention over the world as it is renewable, widely available, cheap and environmental

FUW Trends in Science & Technology Journal, www.ftstjournal.com
e-ISSN: 24085162; p-ISSN: 20485170; December, 2022: Vol. 7 No. 3 pp. 393 - 404

393

friendly (Prahas *et al*., 2008). The focus of this research was to explore the preparation and characterization of activated carbon from these three biomass *Pilliostigma thonningii* (PSH), *Hildergardia barteri* (HB) and *Perqutinia nigrecens* (PNS) and then prepare their composite with magnetite.

Materials and Methods
Sample Collection and Preparation of Adsorbent
Sample collection
The biomass samples used in these study include monkey's bread or camel's foot *(Pilliostigma thonningii),* Kurugbedu (*Hildegardia barteri*), and Agbo *(Perqutinia nigrecens)* fruit shells were collected from farms in Offa local government area of Kwara state, Nigeria.
Preparation of biomass Sample
The samples were cracked using hammer, the seeds embedded in white pulp removed leaving the shells which were needed. The shells were properly washed using de-ionized water to remove dust and impurities deposited on the surface. Dilute nitric acid (0.01M) was also used to wash the shells to further remove impurities, and then rinsed several times with de-ionized water till the pH of the washed water was neutral. The washed shells were air-dried for 5 days under laboratory conditions which was later used to produce activated carbon by a process of carbonization followed by chemical activation. The carbonization process converts the organic materials to primary carbon, whereas the activation process removes the decomposed products deposited in the pores and makes the activated carbon more porous in nature.

Preparation of activated carbon
Carbonization
A 400 g of the sample fruit shells monkey's bread *(Pilliostigma thonningii),* Kurugbedu (*Hildegardia barteri*), and Agbo *(Perqutinia nigrecens)* were carbonized in a pyroliser under a continuous flow of nitrogen gas and at temperatures of 400, 500 and 600 ºC for 60 minutes duration. The charred products were allowed to cool to room temperature, and then crushed using mortar and pestle and stored in air tight containers.

Activation
A 150 g of carbonized sample were weighed and transferred into a beaker containing 150 ml 75% ortho-phosphoric acid (H_3PO_4), ratio 1:1. The impregnation was carried out at 60 ºC in a hot air oven for 24 hrs to achieve well penetration of chemicals into the interior of the precursor. The activated sample was then cooled to room temperature, washed with de-ionized water to neutral pH, oven dried, crushed and stored for characterization. After cooling, each of the carbonized materials was weighed to determine percentage yield per mass of raw sample used (Adebayo *et al.,* 2014).

Magnetite Synthesis
An accurately weighed 80 g sample of $FeSO_4.7H_2O$ was dissolved in 560 ml of deionized water which has been previously flushed with N_2 gas. The glass reactor vessel (1 L) was tightly closed with an air tight plastic lid having holes for insertion of N_2 gas inlets, a thermometer and a dropping funnel. The reactor vessel was placed in a water bath at a temperature of 90 0C and a thermometer was inserted for temperature control and a gas inlet for nitrogen

purging. The entire reaction was conducted under nitrogen. 240 ml of an oxygen-free solution containing 6.46 g KNO3 and 44.9 g KOH were added gradually and steadily within approximately 5 minutes through a dropping funnel once the reaction temperature was reached. After addition of this solution, the mixture was heated for another 60 min and allowed to cool overnight (Cornell and Schwertmann, 1996).
The precipitated samples (black residue) was then washed with deionized water, filtered to obtain black residue, which was then dried in a desiccator and stored in a sample bottle prior to analysis (Cornell and Schwertmann, 1996).

Preparation of magnetite-biomass composite mixture
A 40 g sample of $FeSO_4.7H_2O$ was carefully weighed and dissolved in 280 ml of deionized water which has been previously flushed with N_2 gas. The glass reaction vessel (1 L) was tightly closed with an air tight plastic lid having holes for insertion of N_2 gas inlets, a thermometer and drop funnel. The reaction vessel was placed in a water bath at a temperature of 90 ⁰C and a thermometer was inserted for temperature control and a gas inlet for nitrogen purging. The whole reaction was carried out under nitrogen. Once the reaction temperature was reached, 120 ml of an oxygen-free solution containing 6.46 g KNO_3 and 44.9 g KOH was added gradually and steadily within approximately 5 min through a dropping funnel. After addition of this solution, the mixture was heated for another 60 min and allowed to cool overnight (Cornell and Schwertmann, 1996)
Then, 5 g of biomass powder was added to the mixture, stirred and heated for another 10 min to produce magnetite-biomass ratio 2:1 composite mixture. The same procedure was repeated to synthesize magnetite-biomass ratio 1:1 composite mixture whereby 10 g of biomass powder was used and magnetite-biomass ratio of 1:2 whereby 20 g of biomass powder was used for constant mass of magnetite. All prepared samples were stored in plastic vials and kept in a dessicator prior to analysis.

Determination of Point of zero charge of magnetite
By using the pH drift method (Jai *et al.,*2002), the pH at the point of zero charge (pHpzc) of the adsorbents were measured by adjusting the pH of the solution of 0.1 M KCl between 2 and 12 using 0.01 M HCl/0.01 M NaOH. A 0.05 g of each of the adsorbents were added into 100 ml of NaCl solution in a flask and corked, to eliminate any contact with air and then left for 24 hr at ambient temperature. The final pH was the recorded after the pH had stabilized (after 24 hr). The pH at the point of zero charge (pHpzc) were determined by plotting the graph of pH difference,(∆pH) versus initial pH. The point at which initial pH equals the final pH was taken as the pHpzc of the adsorbent.

Characterization of Adsorbents
The adsorbent moisture content was determined by oven dry method at 105ºC (Hesse, 1997), the ash content by ASTM (ASTM D2866), Bulk density by using density bottle (Yoshiguki and Yukata, 2003), the pH by American Society for Testing and Materials (ASTM D3838, 1996), and the iodine number by ASTM procedure (ATSM D4607). The carbon, hydrogen and nitrogen were analysed by CHN CE 440 analyser and the surface functional groups by Nicolet IS 5 series model FTIR. The particle size morphology and shape of the adsorbent particles was determined using Tenco LV 400 scanning electron

FUW Trends in Science & Technology Journal, www.ftstjournal.com
e-ISSN: 24085162; p-ISSN: 20485170; December, 2022: Vol. 7 No. 3 pp. 393 – 404

394

microscope (SEM). Perkin Elmer C624 was used to determine the elemental composition of the samples by energy dispersive X-ray (EDX) analysis. The nano-particle size was determined using nanosizer and the surface area of the adsorbent was determined by BET method

Results and Discussions
Carbonization Process

Table 1 Carbonization time and temperature for HB, PSH and PNS.

Sample Code	HBa	HBb	HBc	PSHa	PSHb	PSHc	PNSa	PNSb	PNSc
Charring Temperature(^{o}C)	400	500	600	400	500	600	400	500	600
Charring Time (min)	60	60	60	60	60	60	60	60	60
%Yield	23.98	18.10	17.20	32.04	31.44	29.40	32.12	30.60	28.70

Key: HB = *Hildegardia barteri,* PSH = *Pilliostigma thonningii* , PNS = *Perqutinia nigrecens.*

The effects of charring temperature and time which seriously influenced the surface area, yield of adsorbent and bulk density were studied. These physicochemical properties are means to know whether experimental charred carbon can be of use commercially or not (Losso *et al*., 2002). Physicochemical properties describe the suitability of adsorbent for a particular process (Seo *et al.,* 2006). Percentage yield is an important parameter that is used to ascertain the rate of carbonization process. A high yield is required for a feasible economic production of activated carbon. Results for percentage yield of char during various conditions are shown in Table 1. It was observed that there is a direct relationship between charring temperature and percentage yield. The highest percentage yield was attained at 400°C and 60 min for all the three samples. This is because increasing time and / or increasing temperature of carbonization resulted in more volatile component being lost and hence decreasing percentage yield (Abechi *et al.,*2013a). The highest observable percentage yield for HB, PSH, and PNS was 23.98, 32.04 and 32.12% respectively at 400 ^{o}C for 60 min while the least was at 600 ^{o}C for 60 min and the yield was 17.20, 29.40 and 28.70% respectively for HB, PSH and PNS. The negative effect of carbonization

temperature and time was most felt at the highest experimental temperature of 600 ^{o}C (Dina *et al*., 2012).
Physico-Chemical Characteristic of Adsorbent (Biomass)
The physico-chemical characteristic of the adsorbent (a) with carbonization time of 60 min and 400 ^{o}C temperature is presented in Table 2. The moisture content was approximately the same for the three biomass. The moisture content ranges from 0.22 ± 0.03 – 0.44 ± 0.01 % which was lower than banana empty fruit bunch (BEFB), 5.21 ± 0.16% (Sugumaran *et al*,2012). The % ash was higher in *Perqutinia nigrecens* (PNS) (4.20 ± 0.03%) than *Pilliostigma thonningii* (PSH) (3.40 ± 0.02%) and *Hildegardia barteri* (HB) (2.80 ± 0.02%) but all was lower than banana empty fruit bunch (15.73 ± 1.66%) (Sugumaran *et al,* 2012).The ash content is a reflection of the amount of inorganic substituents present, and the higher the value, the higher the value of inorganic constituents. The ash content was within the range of most AC from agricultural products 0.2 – 13.4 % (Ioannidou and Zabaniotou, 2007). The % carbon yield was higher for PSH 41. 61 $\pm$ 0.04 than HB 40.09 $\pm$ 0.04, while PNS 29.40 $\pm$ 0.03 for was the least

Table 2: Physico-chemical characteristic of adsorbent (%wt) dry basis.

| Parameter	PSH	PNS	HB
Moisture (%)	0.33 ± 0.01	0.44 ± 0.01	0.22 ± 0.03
Ash (%)	3.40 ± 0.02	4.20 ± 0.03	2.80 ± 0.02
Carbon yield (%)	41.61 ± 0.04	29.40 ± 0.03	40.09 ± 0.04
Bulk Density (g/ml)	0.635 ± 0.01	0.636 ± 0.01	0.450 ± 0.02
Iodine Number (mg/g)	850.0 ± 10	900.0 ± 20	950.0 ± 25
pH	5.70	6.50	4.40

Bulk density is an important characteristic of the carbon and is invariably related to the starting material. In this study (PNS) *Perqutinia nigrecens* had a higher bulk density of 0.636 $\pm$ 0.01 g/ml than KOH treated DRFP (0.46g/ml) but that of *Hildegardia barteri* (HB) (0.450 $\pm$ 0.01g/ml) was comparable to KOH treated DRFP (Sugumaran *et al,*

2012). The bulk density shows that the precursor 's fiber quality, the lower the weight, the better for its regeneration after use (Abdus-Salam and Buhari, 2014). A sample's iodine number is expressed as the proportion of iodine adsorbed per gram of the sample. The iodine amount of HB (950 $\pm$ 25 mg / g) was found to be higher than that of PNS

FUW Trends in Science & Technology Journal, www.ftstjournal.com
e-ISSN: 24085162; p-ISSN: 20485170; December, 2022: Vol. 7 No. 3 pp. 393 – 404

395

(900 + 20 mg / g) and PSH (850 + 10 mg / g). This may be because HB is more porous than both of them. Activation process increases the surface area and porosity as well as lowering the surface acidity of the activated carbon, which gives rise to low pH values of 4.4 and 5.7 observed for HB and PSH respectively.

Point of zero charge (pHpzc) of Pilliostigma thonningii (PSH), Perqutinia nigrecens (PNS) and Hildegardia barteri (HB) Activated Carbon

The point of zero charge (pHpzc) is the pH at which the effective positive and negative charges on the surface of the adsorbent become zero. The point of zero charge (pHpzc) of the three adsorbents was determined by pH drift method which gave pHpzc for HB as 7.5, PSH as 4.1 and PNS as 4.9. The value for HB was in close agreement with natural goethite (7.8) obtained by Abdus-Salam and Adekola (2005) and also in agreement with that obtained by Nassar and Ringsred (2011) (7.5 $\pm$ 0.5), on goethite nano-adsorbent. The pHpzc is the pH at which the net charge on the surface of the adsorbent is zero. The adsorbents surface charge is positive at pH values lower than the pHpzc and will favour adsorption of negatively charged species but its surface is negatively charged at pH higher than pHpzc, except there are other inter-playing factors. When the surface has net negative charge, it favours adsorption of positively charged species. The pHpzc for *pilliostigma thonningii* and *Perqutinia nigrecens* are in the acidic region while *Hildegardia barteri* in the basic region. The graphs of the pHpzc are shown in the Figs. 1(a, b, and c).

Fig 1a Graph of pHpzc for HB

Fig 1b Graph of pHpzc for PNS

Fig 1c Graph of pHpzc for PSH
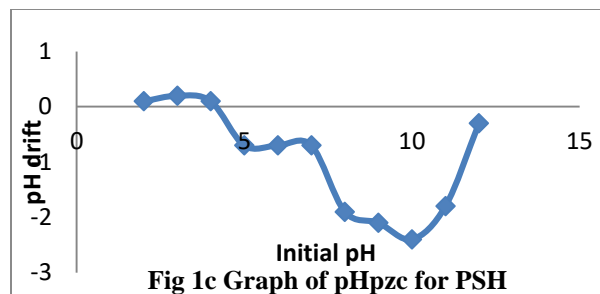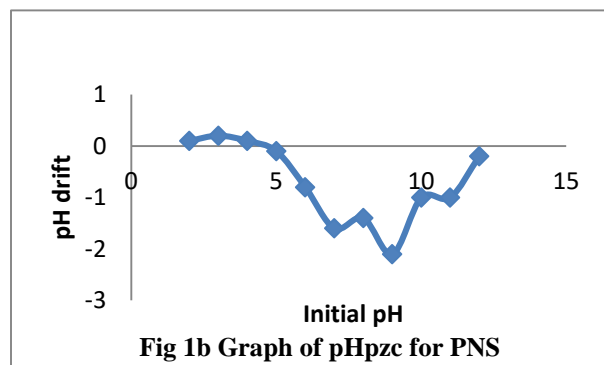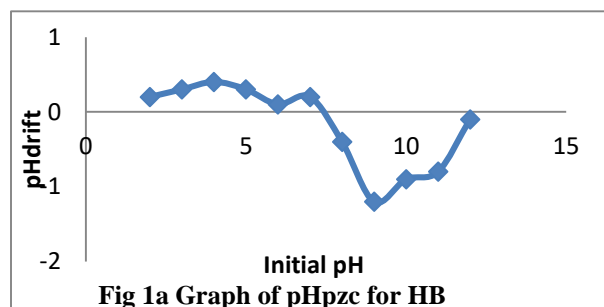
Table 3: CHN Analysis

Biomass	%C	%H	%N
PNS	68.42	3.71	3.42
PSH	69.42	3.34	2.06
HB	72.27	2.82	1.20

Key: PNS=*Perqutinia nigrecens* ; PSH = *Pilliostigma thonningii* ; HB = *Hildegardia barteri*

The CHN analysis was carried out in MEDAC LTD, Alpha 319, Chobham Business Centre, Chertsey Road, Chobham, GU248JB, United Kingdom, using CHN CE 440 analyser. The result is presented in Table 3. The result shows that HB has the highest percentage carbon of 72.27% and PNS the least of 68.42%. PNS has the highest percentage hydrogen and nitrogen of 3.71 and 3.42% respectively. HB has the least value of hydrogen 2.82% and nitrogen 1.20% .The value for carbon was within the range reported for most agricultural materials (41.23 – 84.50 %), hydrogen was below the range(4.63 - 6.26%) while nitrogen was within the range (0.7 – 4.10%) (Ioannidou and Zabaniotou, 2007). The carbon, hydrogen and nitrogen content of PNS was higher than that of mango seed (carbon 52.31%, hydrogen 3.38% and nitrogen 1.02%) while PSH and HB were higher in carbon and nitrogen but lower in hydrogen than mango seed (Abdus-Salam and Buhari, 2014).

Scanning Electron Microscopy

The scanning electron microscopy was carried out using Tenco LV 400 scanning electron microscope, in order to determine the particle size morphology and shape of the adsorbents particles (Harikumar and Joseph,2012). The result obtained from the analysis at different magnification (1,000x and 50,000x) are presented in Figs 2a – 2c. The samples particles showed dense irregular leaf-like shape which tends to agglomerate, smaller and homogenous particles were also found in PSH 1000x magnification. The surface of the PNS particles showed larger pores (high porosity). These pores will be readily available for composite formation with other adsorbents or adsorption process making the sample to have prospect in practical

FUW Trends in Science & Technology Journal, www.ftstjournal.com
e-ISSN: 24085162; p-ISSN: 20485170; December, 2022: Vol. 7 No. 3 pp. 393 – 404

396

application to adsorption process. The 50,000x magnification of the samples showed agglomeration in a sheet-like structures comparable to treated and untreated BEFB (Sugumaran *et al.,*2012).

Fig 2d – 2g are the clear images of the magnetite and the composite particles at different magnifications. The magnetite particles showed dense, irregular shaped and thickly dispersed iron oxide which tends to agglomerate. Smaller and more homogeneous particles were also found in both the magnetite and composite. The surface of the magnetite particles showed larger pores (high porosity), which was also observed in a similar work by Sugumaran *et al.,*2012. These pores will be readily available for a compositing materials (in composite preparation) or

adsorbates (adsorption processes), making magnetite to have to have good practical applicability in adsorption processes (Harikumar and Joseph, 2012).

In a similar manner, the composite particles of the biomass and the magnetite contained dense iron oxide, irregular shapes, heterogeneous and porous surface but the size of pores was found to be reduced compared to the magnetite. This is due to the pores of the magnetite particles being occupied by the biomass activated carbon during the formation of the composite which gives it some distinct characteristics different from both the magnetite and biomass activated carbon. This is a major peculiarity and uniqueness of composites (Abechi *et al*., 2013b).
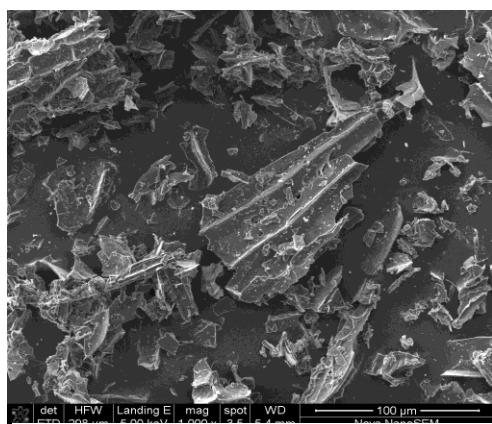

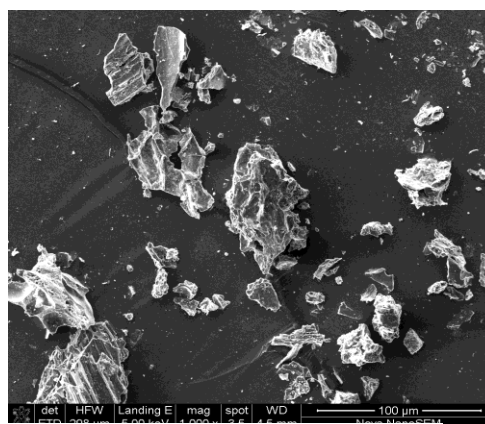Fig 2a:SEM micrograph of *Hildegardia nigrecens* (PNS) particles (mag x 1000x)

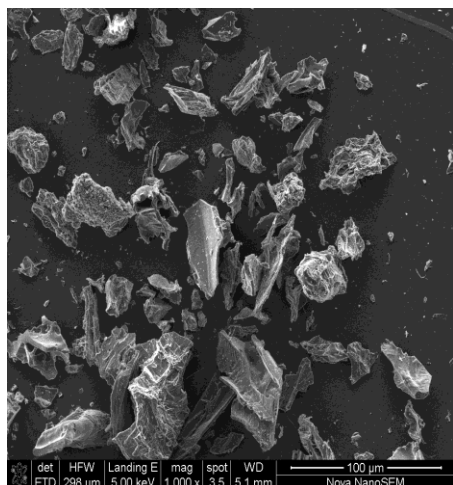Fig.2b: SEM micrograph of *Perqutinia barteri* (HB) particles (mag x1000x)

Fig 2c: SEM micrograph of *Pilliostigma HB composite particles (mag x 20,000x)*
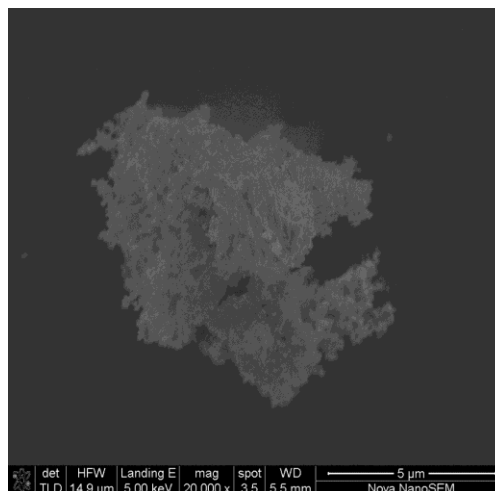

Fig 2d: SEM micrograph of magnetite-*thonningii* (PSH) particles (mag x 1000x

FUW Trends in Science & Technology Journal, www.ftstjournal.com
e-ISSN: 24085162; p-ISSN: 20485170; December, 2022: Vol. 7 No. 3 pp. 393 – 404
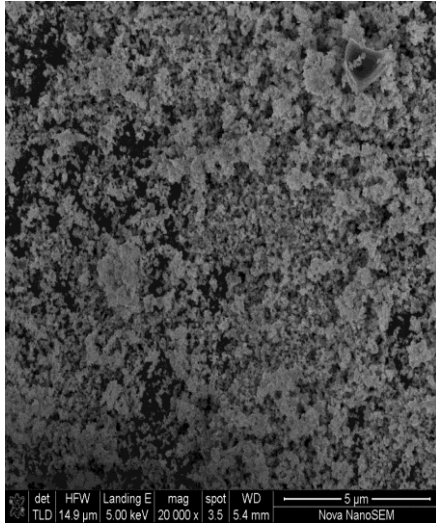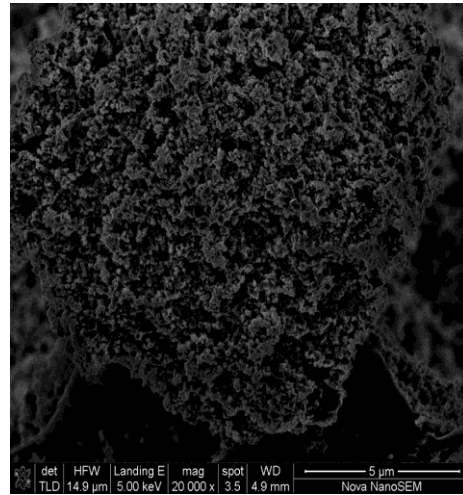
397

Fig2e: SEM micrograph of magnetitePSH composite particles (mag x 20,000x)

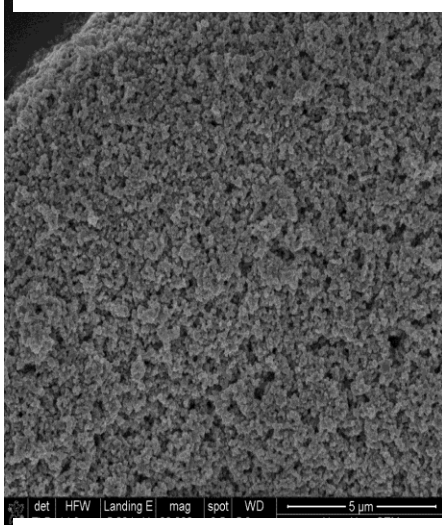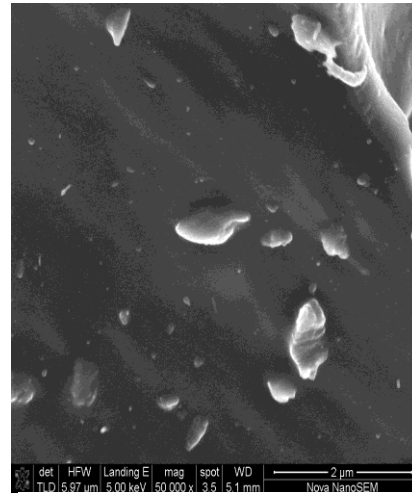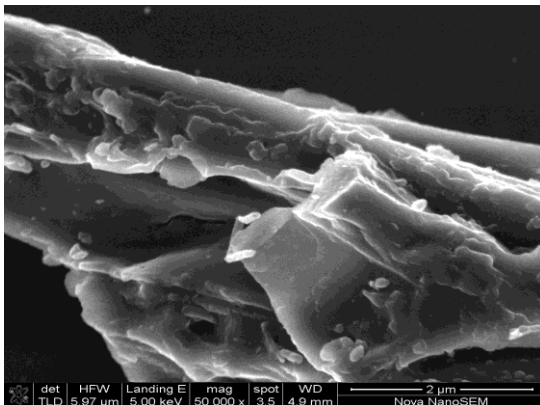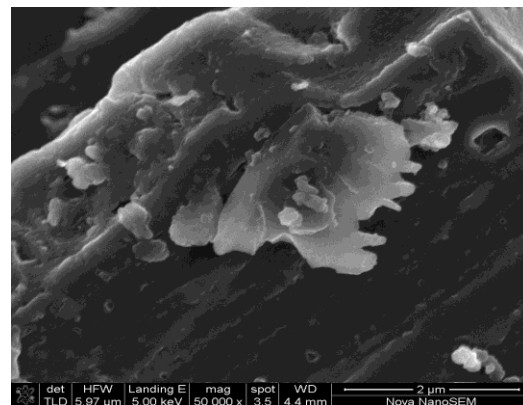Fig 2f: SEM micrograph of magnetite– PNS composite particles (mag x 20,000x)

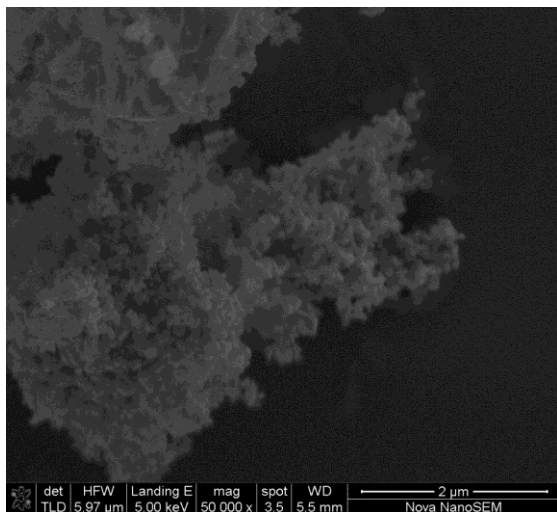Fig 2g: SEM micrograph of *barteri* (HB) particles (mag x 50,000X)

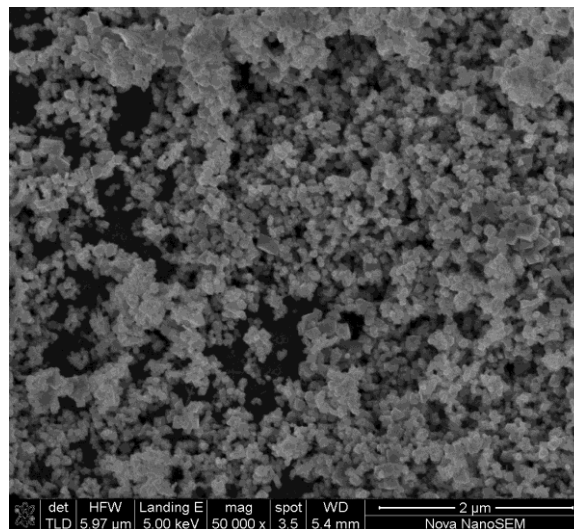App 1a: SEM micrograph of *Hildegardia* particles (mag x 20,000x)

App 1b: SEM micrograph of *Perqutinia* App *nigrecens* (PNS) particles (mag x 50,000X)
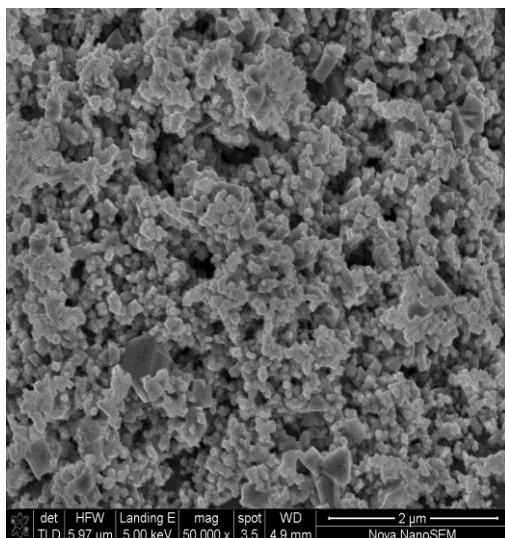

1c: SEM micrograph of *Pilliostigma thonningii (PSH) particles (mag x 50,000X)*

FUW Trends in Science & Technology Journal, www.ftstjournal.com
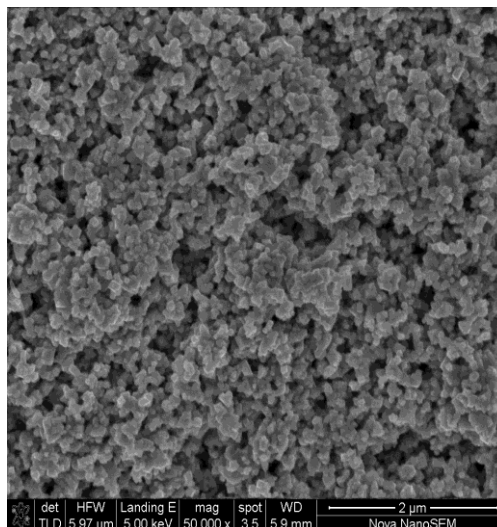e-ISSN: 24085162; p-ISSN: 20485170; December, 2022: Vol. 7 No. 3 pp. 393 – 404

398

App 1d: SEM micrograph of magnetite-composite particles (mag x 50,0000x)

App 1e: SEM micrograph of magnetite- HB composite particles (mag x 50000x)PNS

App 1f: SEM micrograph of magnetite-particles (mag x 50,000x)

App 1g: SEM micrograph of magnetite PSH composite particles (mag x 50,000x)

Energy Dispersive X – Ray (EDX) Analysis

The EDX analysis was carried using Perkin Elmer C624 to determine the elements composition of the sample. Carbon was the predominant element in the samples with 79.20 % for HB, 79.06% for PSH and 76.39 % for PNS. Nitrogen was absent in PSH and HB while it was 5.52 % in PNS. Oxygen was highest in PSH with a value of 20.84 %, followed by HB 20.23 %. The insignificant percentage of phosphorus in HB and PSH appears as impurities. The EDX results for carbon were slightly higher than that of CHN but practically close. The EDX values for carbon ranges from 76.39 – 79.20 % while the CHN ranges from 68.42 – 72.27 %. The values for carbon were within the range reported for most agricultural materials (41.23 – 84.50) (Ioannidou and Zabaniotou, 2007). The higher the carbon content the more desirable the material is as precursor for activated carbon preparation. In the composite, the three major elements were carbon, oxygen and iron (Ioannidou and Zabaniotou, 2007). This result also confirmed the result obtained in FTIR analysis for the composites which show a signal for Fe – O. Carbon ranges from 29.35 % in MPSH to 44.4 % in MPNS, oxygen ranges from 29.52 % in MPSH to 35.56 % in MPNS while iron ranges from 19.55 % in MPNS to 41.13 % in MPSH. Magnetite has the highest percentage of iron (49.57 %) than the composite because of the presence of carbon.

FUW Trends in Science & Technology Journal, www.ftstjournal.com
e-ISSN: 24085162; p-ISSN: 20485170; December, 2022: Vol. 7 No. 3 pp. 393 – 404

399

Table .4: EDX Analysis for activated carbon, composite and magnetite.

| Biomass	%C	%O	%N	%Cl	%S	%P	%Fe	%K
PSH	79.06	20.84	-	-	-	0.1		
PNS	76.39	17.93	5.52	0.16	-	-		
HB	79.20	20.23	-	-	0.22	0.35		
MPSH	29.35	29.52	-	-	-	-	41.13	-
MHB	34.50	34.15	-	-	-	-	30.41	0.94
MPNS	44.40	35.56	-	-	-	-	19.55	0.49
M	14.89	35.55	-	-	-	-	49.57	-

PSH = *Pilliostigma thonningii* , PNS = *Perqutinia nigrecens,* HB = *Hildegardia barteri,* M = Magnetite

Fourier Transform Infrared (FTIR)

The spectra were recorded over the range of 500 – 4000 cm^{-1} using Nicolet IS 5 series FTIR spectrophotometer. The various absorption bands obtained were utilized in the characterization of magnetite particles using reported values (Shu and Wang, 2009) (Table 5a). The analysis indicated absorption peak at 555.15 cm^{-1} corresponding to the Fe-O vibration related to magnetite phase (Mahdavi *et al.,*2013). The broad band 3000 – 4000 cm^{-1} centered at 3563.06 cm^{-1} and 3160.95 cm^{-1} was assigned to O-H stretching and bending vibrations arising from surface hydroxyl groups on magnetite. Two weak absorption bands occurred at 2771.50 cm^{-1} and 2055.94 cm^{-1} in the spectrum corresponds to H-O-H bending and stretching vibration mode (Awwad and Salem, 2012). The strong bands at 1102.90 cm^{-1} and 555.15 cm^{-1} correspond to stretching and bending vibrations of Fe-O bonds typical of the crystalline lattice of magnetite (Hou *et al.,*2003)
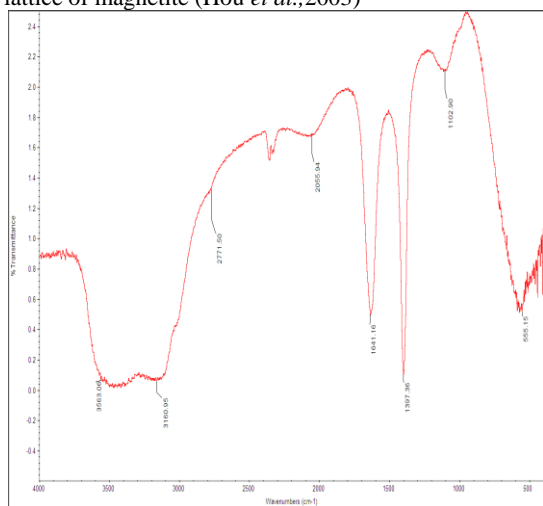
Fig .3a: FTIR spectrum of the *bateri* Activated carbon.
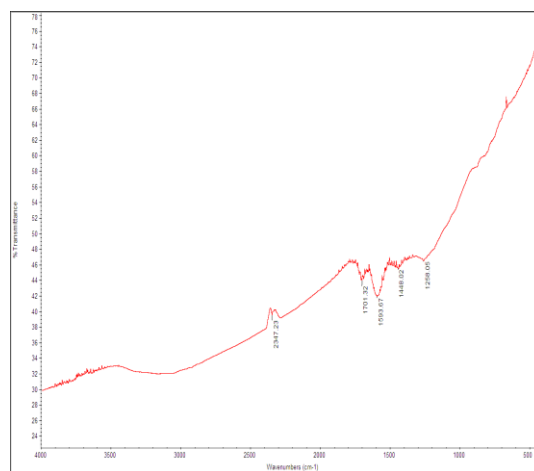
Fig .3b: FTIR spectrum for *Hildergardia* synthesized magnetite

The spectrum of *Hildergardia bateri* was recorded in the range of 500 – 4000 cm^{-1}. The spectra showed prominent peak at 2347.23 cm^{-1} that was attributed to $C \equiv C$ stretching vibration. Peaks were also observed at 1701.32 and 1593. 67 cm^{-1} depicting C = O stretching and conjugated C = C (Abdus-Salam and Buhari, 2014).

The spectrum of *Pilliostigma thonningii* activated carbon was recorded over a range 500 – 4000 cm^{-1} a peak was observed at 2920.32 cm^{-1} which was attributed to C-H asymmetric stretching vibration of CH_2. Other peaks were observed at 2350.40 cm^{-1},1704.49, 1448.02 and 874.93/811.61/748.28 cm^{-1} depicting $C \equiv C$ stretching vibration, C=O stretching, methyl C-H asymmetric/symmetric bend and C-H bending (out of plane) vibration respectively (Coates,2012).

Perqutinia nigrecens activated carbon, the spectrum was recorded over 500 – 4000 cm^{-1}. It shows a prominent peak at 2926.65 cm^{-1} that was attributed to C-H asymmetric stretching vibration of CH_2. A strong absorption was noticed at 2350.40, 1704.49, 1606.33 and 874.93 /783.11 cm^{-1} which indicates $C \equiv C$ stretching vibration, C=O

FUW Trends in Science & Technology Journal, www.ftstjournal.com
e-ISSN: 24085162; p-ISSN: 20485170; December, 2022: Vol. 7 No. 3 pp. 393 – 404

400

stretching, conjugated C = C and C-H bending (out of plane) vibration respectively. For most carbonaceous materials C=C stretching absorption frequently occurs at about 1600 cm^{-1} region (Florido *et al*., 2009)

Table .5a: Summary of the assignments of Peaks of HB, PSH, PNS and Magnetite

HB Frequencies (cm^{-1})	PSH Frequencies (cm^{-1})	PNS Frequencies (cm^{-1})	Magnetite Frequencies (cm^{-1})	Assignment
			3563.06 and 3160.95	O-H Stretching and bending vibration
-	2920.32	2926.65	-	C-H Asymmetric stretching vibration of CH$_2$
-	-	2844.33	-	C-H Stretching vibration of CH$_3$,CH$_2$
2347.23	2350.40	2350.40	-	C≡C Stretching vibration
1701.32	1704.49	1704.49	-	C=O Stretching
1593.67	1596.83	1606.33	-	Conjugated C=C
1441.69 and 1365.70	1448.02	1448.02 and 1372.03	-	Methyl C-H Asymmetric/Symmetric bend
-	874.93/811.61/748.28	874.93/783.11	-	C-H bending (out of plane) vibration
-	-	-	1102.90 and 555.15	Fe-O Stretching and bending vibrations

Table .5b: Summary of the assignments of Peaks of MPN, MPS and MHB.

MPN Frequencies (cm^{-1})	MPS Frequencies (cm^{-1})	MHB Frequencies (cm^{-1})	Assignments
3319.26	-	-	O-H Stretching vibration.
2964.64/2936.15	-	-	C-H Stretching and bending vibration of CH$_2$
2866.49	-	-	C–H Stretching vibration of CH$_3$CH$_2$
2366.23	-	-	C≡C Stretching vibration
-	1626.33	1593.67	Conjugated C=C
1463.85/1378.36/1327.70	-	1378.36	Methyl C-H Asymmetric/Symmetric bend
-	893.93/792.61	890.77	C-H bending (out of plane) vibration
583.64/447.49	586.81/450.66	586.81/450.66	Fe-O Stretching and bending vibrations

Brunauer Emmett Teller Specific Area Determination
The specific surface area (SSA) of the magnetite (MAG), MPSH, MHB and MPNS were determined by the BET adsorption method using nitrogen as the adsorbate. The analysis was carried out using Nova station C BET instrument and the result are summarized in Table 6a.

FUW Trends in Science & Technology Journal, www.ftstjournal.com
e-ISSN: 24085162; p-ISSN: 20485170; December, 2022: Vol. 7 No. 3 pp. 393 – 404

401

The multipoint BET specific surface area of the magnetite (MAG) was found to be 353.5 m²/g, micropore volume and half micropore width were found to be 15.22 cm³/g and 5.842 nm respectively. Multipoint BET surface area for MHB, MPNS, and MPSH, the composites were found to be 574.5, 530.4 and 475.1 m²/g respectively, while their micropore volume and half micropore width were 29.13 and 3.866 , 18.68 and 6.435, 17.35 cm³/g and 6.366 nm respectively. This result made the synthesized (MAG) to fall into the category of 'Ideal crystal' of magnetite (SSA > 80 m²/g) (Villalobos and Perez-Gallegos, 2008). The large difference in the BET surface areas, pore size and pore volume of the magnetite (MAG) and the composite particles are indications that the synthesized magnetite particles are smaller in size than the composite particles due to the incorporation of the larger particles of the biomass activated carbon, leading to the reduced surface area (Villacis-Garcia *et al*., 2015). An excellent performance of the composite in the adsorption studies more than the magnetite particles will be expected due to the increase in the surface reactivity of the composite with the higher surface area brought about by the presence of surface functional groups.

Table .6a: Summary of BET Data for MAG, MHB, MPNS and MPSH

Materials	Multipoint BET Surface Area (m²/g)	Langmuir Surface Area (m²/g)	Micropore Volume (cm³/g)	Micropore Width (nm)	Pore Diameter (nm)
MAG	353.5	1068	15.22	5.852	2.800
MHB	574.5	967.5	29.13	3.866	2.140
MPNS	530.4	8795	18.68	6.435	3.000
MPSH	475.1	4161	17.35	6.366	2.960

Table 6b: BET comparative data for activated carbon, magnetite (MAG) and composite

Materials	Surface Area (m²/g)	Porous total volume (cm³/g)	Porous diameter average (nm)	Reference
Fe₃O₄-SiO₂	82.24	0.42	10.109	Nuryono *et al*., (2014)
Fe₃O₄-SiO₂-SH 50 : 50	162.52	0.48	5.874	"
Fe₃O₄-SH	3.42	0.02	10.894	"
Fe₃O₄	114.0	-	-	Jiahong *et al*., (2010)
Fe₃O₄-SiO₂	318.5	-	-	"
Fe₃O₄-SiO₂-NH₂	216.2	-	-	"
Mucilaginous leaves of *Diceriocaryum eriocarpum* plant	535	-	2.96	Joshua *et al*., (2015)

The surface area of the magnetite obtained were greater than that reported by Nuryono *et al.*,(2014), 82.24, 162.52, and 3.42 m²/g and Jiahong *et al.*, (2010), 114.0, 318.5 and 216.2 m²/g (Table 6b). The surface area signifies that the particles were smaller in size (Villacis-Garcia *et al*., 2015), and smaller than that reported by Nuryono *et al*., (2014), with porous diameter 10.109, 5.874 and 10.894 nm.

Conclusion:
The preparation of PSH, HB and PNS activated carbon was very successful and their ash content was 3.40 ± 0.02, 4.20 ± 0.03 and 2.80 ± 0.02 % for PSH, PNS and HB respectively. The bulk density which is an important characteristic of carbon and is invariably related to the starting material is given as 0.635 ± 0.01, 0.636 ± 0.01 and 0.450 ± 0.02 g/ml for PSH, PNS and HB respectively. The pH_{pzc} was 7.5 for HB, 4.9 for PNS and 4.1 for PSH. Two were in the acidic region while one was in the basic region. The FTIR analysis depicted $C \equiv C$, $C = O$ and $C = C$ conjugated in all the activated carbon, which disappears in the composite signifying formation of composite. The surface area was moderately high in all the composite, giving them a better chance for adsorption.

References
Abdus – Salam, N and Buhari, M., 2014. Adsorption of Alizarin and Fluorescein Dyes on Adsorbent Prepared from Mango Seed". *Pacific Journal of Science and Technology.* **15**(1):232 – 244.

Abdus-Salam, N. and Adekola, F. A. 2005.The Influence of pH and Adsorbent Concentration on Adsorption of Lead and Cadmium on a Natural Goethite, *African Journal of Science and Technology (AJST) Science and Engineering Series,* **6**(2): 55 - 66

Abechi S.E., Gimba, C. E. Uzairu A. and Dallatu Y. A. 2013a. Preparation and characterization of activated carbon from palm kernel shell by chemical activation, *Research Journal of Chemical Sciences,* **3**(7):54 - 61

Abechi,S. E., Gimba, C. E., Uzairu, A., Kagbu,J. A. and Ocholi,O. J. 2013b. Equilibrium Adsorption Studies of Methylene blue onto palm kernel shell- based activated carbon. *International Referreed Journal of Engineering and science,* **2**(5): 38-45.

Adebayo, G. B., Abdus- Salam, N. and Elelu, S. A. 2014. Adsorption of Lead (II) Ions by Activated Carbon Prepared From Different Parts of *Jatropha curcas* Plant.*Ilorin Journal of Science*, **1**(1): 28- 49.

Asiagwu, A. K., Owamah, H.I. and Illoh, V.O. 2012." Kinetic and Thermodynamic Models for the Removal of Amino – phenol (dye) From Aqueous Solutions Using Groundnut *(Arachis hypogea*) Shells as the Biomass". *Advances in Applied Science Research.* **3**(4): 2257-2265.

FUW Trends in Science & Technology Journal, www.ftstjournal.com
e-ISSN: 24085162; p-ISSN: 20485170; December, 2022: Vol. 7 No. 3 pp. 393 - 404

402

ASTM D2866 "Test Method for Total Ash Content of Activated Carbon" In: *2006 Annual Book of ASTM Standard. Vol. 15.01.* American Society for Testing and Materials: West Conshohocken, PA

ASTM D4607. "Test Method for the Determination Iodine Number of Activated Carbon". In: *2006 Annual Book of ASTM Standard Vol. 15.01.* American Society for Testing Materials: West Conshohocken, PA.

Awwad, A.M. and Salem, N.M. 2012. A green and facile approach for synthesis of magnetite nanoparticles, *Nanoscience and Nanotechnology Journal,* **2**(6), 208-213.

Bhatnagar, A. and Sillanpaa, M. 2010. Utilization of Agro – Industrial and Municipal Waste Materials as Potential Adsorbents for Water Treatment- A Review. *Chemical Engineering Journal*, **157**: 277 – 296.

Brookstein, D. S. 2009. Factors Associated with Textile Pattern Dermatitis Caused by Contact Allergy to Dyes, Finishes, Foams and Preservatives Dermatol. *Clin*. 27: 309 – 322.

Chiou, M. S. and Li, H. Y. 2002. Equilibrium and Kinetic Modeling of Adsorption of Reactive Dye on Cross-Linked Chitosan Beads. Journal Hazardous Materials. **93:** 233-248.

Coates, J. 2012. Interpretation of Infrared spectra, A practical Approach. Encyclopedia of Analytical Chemistry. R.A Meyers (Ed) copyright John wiley and Sons Ltd.

Cornell, R.M., and Schwertmann, U., 1996. The iron oxides: Structure, Properties, reaction, occurrences and uses, 2nd edition, New York Wiley-VCH.665.

Dina, D.J.D., Ntieche, A.R., Ndi, J. N. and Ketcha, M. J. 2012. Adsorption of acetic acid onto activated carbons obtained from maize cobs by chemical activation with zinc chloride ($ZnCl_2$). *Research Journal of Chemical Sciences,* **2**(9):42-49.

Florido, A.C., Valderrama, J. A., Arevalo, I.,Casas, M. Martinez and N. Miralles 2009. "Application of Two Sites Non-Equilibrium Sorption Model for the Removal of Cu (II) onto Grape Stalk Wastes in a Fixed-Bed Column" Chemical Engineering Journal **156:**298-304.

Harikumar, P. S. and Joseph, L. 2012.Kinetic and Thermodynamics Studies of As(III) Adsorption onto Iron Nanoparticles Entrapped Ca- Alginate Beads. *International Journal of Plant, Animal and Environmental Sciences* **2**(1): 159 – 166.

Hesse, P.R. 1997. *A Textbook of Soil Chemical Analysis, Illustrated.* Chemical Publish Co. John Murray: London, UK. 520.

Hou, J., Yu, Y., and Gao, S. 2003. Solvothermal Reduction Synthesis and Characterization of Superparamagnetic Magnetite Nanoparticle. *Journal of Materials Chemistry,* **13**, 1983 – 1987.

Ioannidou, O. and Zabaniotou, A. 2007."Agricultural residues as precursor for Activated Carbon Production: A Review" *Renewable and Sustainable Energy Reviews.* 11:1966-2005.

Jai, Y. F., Xiao, B. and Thomas, K. M. 2002. Adsorption of Metal ions on Nitrogen Surface Functional Groups in Activated Carbons *Lanmnuir*, **18:** 470 – 478.

Jiahong, W., Shourong, Z., Yun, S., Jingliang, L. Zhaoyi, X. and Dongqiang, Z. 2010.Amino-functionalized $Fe_3O_4@SiO_2$ core-shell magnetic nanomaterial as a novel adsorbent for aqueous heavy metals removal. *Journal of colloid and interface science,* **349**: 293-299.

Joshua, E. N.,Odiyo, J. O., Msagati, T. A., and Popoola, E. O., 2015. A Novel Approach for the removal of lead (II) ion from wastewater using mucilaginous leaves of diceriocaryum eriocarpum plant. *Sustainability*, **7**(10): 14026-14041.

Lima, R. O. A., Bazo, A. P., Salvadori, D. M. F., Rech, C. M. Olivera, D. P. and Umbuzeiro, G. A. 2007. Mutagenic and Carcinogenic Potential of a Textile Azo – dye Processing Plant Effluent that Impacts a Drinking Water Source. *Mutat. Res. Genet. Toxicol. Environ. Mutagen.* **626**: 53 - 60

Losso N.J., Ng, C. Marshall, E. M. and Rao, M. R. 2002. Physical and chemical properties of agricultural by-product based activated carbons and their ability to adsorb geosmin. *Bioresources and Technology,* **84:**177 – 185.

Mahdavi, M., Ahmad, M.B., Haron, M.J., Gharayebi, Y., Shameli, K. and Nadi, B. 2013. Fabrication and characterization of SiO_2 / (3-Aminopropyl) triethoxysilane-coated magnetite nanoparticles for lead(II) removal from aqueous solution. *Journal of Inorganic and Organometallic Polymer,* **23,** 599-607

Nassar, N. N. and Ringsred, A. 2011. Rapid Adsorption of Methylene Blue from Aqueous Solution by Goethite Nano-adsorbents. *Environmental Engineering Science*. **29**(8):790 – 797.

Nuryono, N., Nur, M. R., Bambang, R., Satya, C.W.S., and Shunitz, T.2014. Coating of magnetite with mercapto modified rice hull ash silica in a one-pot process, *Springer plus*, **3**:3-15.

Paul, J. Rawat, K. P., Sarma, K. S. S. and Sabharwal, S. 2011. Decoloration and Degradation Reactive Red – 120 Dye by Electron beam Irradiation in Aqueous Solution. *Applied Radiation Isotopes.* 69: 982 – 987.

Prahas, D. Kartika, Y., Indraswati, N. and Ismadji, S. 2008. Activated Carbon from Jackfruit Peel waste by H_3PO_4 Chemical Activation: Pore Structure and Surface Chemistry Characterization. *Chemical Engineering Journal.* **140**: 32 – 42.

Rosa, S, Laranjeira, M. C. M., Riela H. G. and Favere, V. T. 2008. Cross-Linked Quaternary Chitosan as an Adsorbent for the Removal of the Reactive Dye from Aqueous Solutions. *Journal of Hazardous Materials*. **155**: 253 –260.

FUW Trends in Science & Technology Journal, www.ftstjournal.com
e-ISSN: 24085162; p-ISSN: 20485170; December, 2022: Vol. 7 No. 3 pp. 393 – 404

403

Royer, B. Cardoso, N.F., Lima, E. C. Macedo, T.R. and Airoldi, C .2010. A Useful Organofunctionalized Layered Silicate for Textile Dye Removal. *Journal of Hazardous Materials*. **181**: 366 – 374.

Royer, B., Cardoso, N. F. Lima, E. C., Vaghetti, J. C. P., Simon, N. M., Calvete, T. and Veses, R. C. 2009. Application of Brazilian-pine Fruit Shell in Natural and Carbonized Forms as Adsorbents to Removal of Methylene Blue from Aqueous Solutions – Kinetic and Equilibrium Study. *Journal of Hazardous Materials.* **164**: 1213 – 1222.

Seo W.C., Kermit, W., Yang, H., and Marshall E. W.,2006. Selected metal adsorption by activated carbon made from peanut shells, *Bioresources and Technology*, **97**:2266-2270 .

Shu, Z. and Wang, S. 2009. Synthesis and characterization of magnetic Fe_3O_4 / MnO_2 composite particles. *Journal of nanomaterials*, 1-5

Sugumaran, P. ,Priya, S.V. , Ravichandran, P. , and Seshadri, S.2012.Production and Characterization of Activated Carbon from Banana Empty Fruit Bunch and *Delonix regia* Fruit Pod. *Journal of Sustainable Energy and Environment* **3**(2012):125 – 132.

Torregrosa-Macia, R., Martin- Martinez, J.M. and Mittelmeijer-Hazeleger, 1997. "Porous Texture of Activated Carbons Modified with Carbohydrates" *Carbon* **35**(4): 447 – 453.

Villacis-Garcia M., Ugalde-Arzate M., Vaca-Escobar K., Villalobo-Rodolfo M. Z. and Martinez-Villegas N. 2015. Laboratory synthesis of goethite and ferrihydrite of control particle sizes. *Boletin De la Sociedad Geologica Mexicana,* **67**(3): 433- 446.

Villalobos M. and Perez-Gallegos A. 2008. Goethite surface reactivity: A macroscopic investigation unifying proton, chromate, carbonate and lead (II) adsorption. *Journal of Colloid and Interface Science,* **326**: 307-323.

Wang, X.S., Zhou, Y., Yiang, Y. and Sun, C. 2008. The Removal of Basic Dyes from Aqueous Solutions Using Agricultural By-products. *Journal of Hazardous Materials*. **157**: 374 – 385.

Yoshiguki, S. and Yukata, K. 2003. "Pyrolysis of Plant, Animal and Human Waste: Physical and Chemical Characterization of the Pyrolytic Product". *Bioresource Technology*. **90**(3): 241 - 247

FUW Trends in Science & Technology Journal, www.ftstjournal.com
e-ISSN: 24085162; p-ISSN: 20485170; December, 2022: Vol. 7 No. 3 pp. 393 – 404

404